processes can be stimulated in an analogous manner to inelastic scattering in our experiment—by using a precursor molecule (such as HCl) and forcing 're-collision' between a proton and the heavy nucleus with an intense few-cycle optical pulse. To follow the subsequent dynamics, the relative trajectories of the correlated, charged nuclear fragments, as influenced by the field, can be measured.

Regarding the 'probe', we note that any method of observing the relative evolution of the correlated particles can be used for measurement. In molecular science, harmonic generation is one possible method[16] where phase matching eliminates the contribution from all but the first electron wave packet return, which occurs about two-thirds of a period following ionization. Elastic scattering is a second possible method[6], with diffraction determining the nuclear position at the time of re-collision. □

Methods

Production and control of the electron wave packet

An optical parametric amplifier is used to shift the 40-fs output of a Ti:sapphire laser system to longer wavelengths. We use 800 nm, 1.2 μm, 1.53 μm and 1.85 μm pulses. Each ionizes D_2 near the field maximum and provides a progressively longer time delay between ionization and re-collision. Taking the peak of the first electron microbunch to be the delay time, this corresponds to delay times of 1.7, 2.7, 3.4 and 4.2 fs. Changing the wavelength has other implications. The intensity and wavelength determine the maximum re-collision energy $3.17q^2E^2/(4m\omega^2)$ of the electron[7] (q and m are the electron mass and charge, ω and E are the laser pulse's angular frequency and electric field amplitude at the time of ionization). We use a light intensity of 1.5×10^{14} W cm^{-2}, calibrated against the ionization of xenon. Whereas at 800 nm the peak kinetic energy of the re-colliding electron is 30 eV, the ω^{-2} scaling of the kinetic energy means that at 1.85 μm the energy of the peak re-colliding electron is about 160 eV.

Kinetic energy analysis

The kinetic energy spectrum of D^+ was measured with a time-of-flight (TOF) mass spectrometer filled with 10^{-6} torr of D_2. The TOF axis was perpendicular to the direction of propagation of the laser beam. A 1-mm-diameter hole in the electrode placed 1.5 cm from the laser focus selects only those D^+ ions resulting from dissociation of D_2^+ molecules that are aligned along the TOF axis. For the high-resolution results taken with 800-nm light (not shown), the extraction field was 133 V cm^{-1} and the acceptance angle of the TOF was 6 degrees at 8 eV. For the lower-resolution results, the extraction field was 400 V cm^{-1} giving an acceptance angle of 9 degrees at 8 eV.

Selection of the re-collision channel

Deuterium ions are produced by a number of processes during strong field ionization of D_2. We distinguish fragments resulting from inelastic scattering caused by the returning electron (Fig. 2) from those produced by any other process (such as sequential double ionization[22], bond softening[23] and enhanced ionization[24–27]) using the strong sensitivity of recollision phenomena to the ellipticity of the light polarization[6,7,13]. It only takes a small ellipticity to displace the electron laterally with respect to the parent ion so recollision is impossible[7]. In strong fields, the difference between the spectrum obtained with linear and elliptically polarized light is due to recollision.

Received 24 July 2002; accepted 13 January 2003; doi:10.1038/nature01430.

1. Drescher, M. *et al.* Time-resolved atomic inner-shell spectroscopy. *Nature* **419,** 803–807 (2002).
2. Hentschel, M. *et al.* Attosecond metrology. *Nature* **414,** 509–513 (2001).
3. Paul, P. M. *et al.* Observation of a train of attosecond pulses from high harmonic generation. *Science* **292,** 1689–1692 (2001).
4. D'Ariano, G. M., Presti, P. L. & Paris, M. G. A. Using entanglement improves the precision of quantum measurements. *Phys. Rev. Lett.* **87,** 27040 (2001).
5. Resch, K. J., Lundeen, J. S. & Steinberg, A. M. Experimental observation of nonclassical effects on single-photon detection rates. *Phys. Rev. A* **63,** 020102 (2000).
6. Niikura, H. *et al.* Sub-laser-cycle electron pulses for probing molecular dynamics. *Nature* **417,** 917–922 (2002).
7. Corkum, P. B. Plasma perspective on strong field multiphoton ionization. *Phys. Rev. Lett.* **71,** 1994–1997 (1993).
8. Dietrich, P., Burnett, N. H., Ivanov, M. & Corkum, P. B. High harmonic generation and correlated two-electron multiphoton ionization with elliptically polarized light. *Phys. Rev. A* **50,** 3585–3588 (1994).
9. Paulus, G. G., Nicklich, W., Xu, H., Lambropoulos, P. & Walther, H. Plateau in above threshold ionization spectra. *Phys. Rev. Lett.* **72,** 2851–2854 (1994).
10. Weber, Th. *et al.* Correlated electron emission with multiphoton double ionization. *Nature* **405,** 658–661 (2000).
11. Bhardwaj, V. R., Rayner, D. M., Villeneuve, D. M. & Corkum, P. B. Quantum interference in double ionization and fragmentation of C_6H_6 in intense laser fields. *Phys. Rev. Lett.* **87,** 253003 (2001).
12. Zewail, A. H. Femtosecond chemistry. *Science* **242,** 1645–1653 (1988).
13. Krause, J. L., Schafer, K. J. & Kulander, K. C. High-order harmonic generation from atoms and ions in the high intensity regime. *Phys. Rev. Lett.* **68,** 3535–3538 (1992).
14. Lewenstein, M., Balcou, Ph., Ivanov, M. Yu., L'Huillier, A. & Corkum, P. B. Theory of high-harmonic generation by low-frequency laser fields. *Phys. Rev. A* **49,** 2117–2132 (1994).
15. Ivanov, M., Corkum, P. B., Zuo, T. & Bandrauk, A. Routes to control of intense-field atomic polarizability. *Phys. Rev. Lett.* **74,** 2933–2936 (1995).
16. Lein, M., Hay, N., Velotta, R., Marangos, J. P. & Knight, P. L. Role of the intramolecular phase in high-harmonic generation. *Phys. Rev. Lett.* **88,** 183903 (2002).
17. Hargittai, I. & Hargittai, M. *Stereochemical Applications of Gas-Phase Electron Diffraction* (VCH, New York, 1998).
18. Yudin, G. L. & Ivanov, M. Yu. Physics of correlated double ionization of atoms in intense laser fields: Quasistatic tunneling limit. *Phys. Rev. A* **63,** 033404 (2001); erratum **64,** 019902 (2001).
19. Peek, J. M. Inelastic scattering of electrons by the hydrogen molecule ion. *Phys. Rev. A* **134,** 877–883 (1964).
20. Schinke, R. *Photodissociation Dynamics* 114–115 (Cambridge Univ. Press, Cambridge, UK, 1993).
21. Itatani, J. *et al.* Attosecond streak camera. *Phys. Rev. Lett.* **88,** 173903 (2002).
22. Lambropoulos, P. Mechanisms for multiple ionization of atoms by strong pulsed lasers. *Phys. Rev. Lett.* **55,** 2141–2144 (1985).
23. Zavriyev, A., Bucksbaum, P. H., Muller, H. G. & Schumacher, D. W. Ionization and dissociation of H_2 in intense laser fields at 1.064 μm, 532 nm, and 355 nm. *Phys. Rev. A* **42,** R5500–R5513 (1990).
24. Codling, K. & Frasinski, L. J. Dissociative ionization of small molecules in intense laser fields. *J. Phys. B* **26,** 783–809 (1993).
25. Seideman, T., Ivanov, M. Yu. & Corkum, P. B. Role of electron localization in intense-field molecular ionization. *Phys. Rev. Lett.* **75,** 2819–2822 (1995).
26. Zuo, T. & Bandrauk, A. D. Charge-resonance-enhanced ionization of diatomic molecular ions by intense lasers. *Phys Rev. A* **52,** R2511–R2514 (1995).
27. Constant, E., Stapelfeldt, H. & Corkum, P. B. Observation of enhanced ionization of molecular ions in intense laser fields. *Phys. Rev. Lett.* **76,** 4140–4143 (1996).

Acknowledgements We acknowledge discussions with A. Stolow, A. Sokolov, A. D. Bandrauk, S. Chelkowski and J. Marangos. The authors appreciate financial support from Canada's Natural Science and Engineering Research Council, the Canadian Institute for Photonics Innovation, and Le Fonds Québécois de la Recherche sur la Nature et les Technologies.

Competing interests statement The authors declare that they have no competing financial interests.

Correspondence and requests for materials should be addressed to P.B.C. (e-mail: Paul.Corkum@nrc.ca).

Multi-colour organic light-emitting displays by solution processing

C. David Müller*†, Aurélie Falcou‡, Nina Reckefuss*†, Markus Rojahn§, Valèrie Wiederhirn§, Paula Rudati*†, Holger Frohne*†, Oskar Nuyken§, Heinrich Becker‡ & Klaus Meerholz*†

** Department Chemie, Universität München, Butenandtstr. 11, 81377 München, Germany*
‡ Covion Organic Semiconductors GmbH, Industriepark Hoechst, G865, 65926 Frankfurt, Germany
§ Lehrstuhl für Makromolekulare Stoffe, Technische Universität München, Lichtenbergstr. 4, 85747 Garching, Germany

Organic light-emitting diodes (OLEDs) show promise for applications as high-quality self-emissive displays for portable devices such as cellular phones and personal organizers[1–4]. Although monochrome operation is sufficient for some applications, the extension to multi-colour devices—such as RGB (red, green, blue) matrix displays—could greatly enhance their technological impact. Multi-colour OLEDs have been successfully fabricated by vacuum deposition of small electroluminescent molecules, but solution processing of larger molecules (electroluminescent polymers) would result in a cheaper and simpler manufacturing process. However, it has proved difficult to combine the solution processing approach with the high-resolution patterning techniques required to produce a pixelated display. Recent attempts have focused on the modification of standard printing techniques, such as screen printing[5–7] and ink jetting[8], but those still have technical drawbacks. Here we report a class of electroluminescent polymers that can be patterned in a way similar to standard photoresist materials—soluble polymers with oxetane

† Present address: Institut für Physikalische Chemie, Universität zu Köln, Luxemburgerstr. 116, 50939 Köln, Germany.

sidegroups that can be crosslinked photochemically to produce insoluble polymer networks in desired areas. The resolution of the process is sufficient to fabricate pixelated matrix displays. Consecutive deposition of polymers that are luminescent in each of the three RGB colours yielded a device with efficiencies comparable to state-of-the-art OLEDs and even slightly reduced onset voltages.

Small-molecule OLEDs are commonly fabricated by vacuum deposition, whereas polymer OLEDs are usually built by solution processing (mostly spin-coating). The latter route has the advantage of much easier device manufacture, and efficient single-layer devices with low turn-on voltages can be obtained. By contrast, vacuum deposition allows for the fabrication of multiple-layer devices, which are generally more efficient than their single-layer analogues. Furthermore, by using shadow masks, patterned structures can be obtained. Recent research efforts focus on the adaptation of printing techniques such as screen printing[5,6] and ink jetting[8] to polymer OLED technology. Screen printing has been demonstrated as a simple patterning method to obtain macro-structured two-colour signs. However, owing to its accuracy limitations, it can currently not be used for full-colour display fabrication. Ink jet printing on the other hand offers the possibility of achieving high resolution, but has the disadvantage that the wettability of the substrate has to be pre-adjusted (patterned by photoresist technique) in order to place the drops at the precise location (wetting of pixel, but not of bank). Often inhomogeneous films are obtained after drying. In addition, the alignment of drops in consecutive depositions is a rather cumbersome process; for example, the deposition of an electroluminescent (EL) polymer on top of the commonly used hole-injecting polymer PEDOT (poly(3,4-ethylenedioxy-thiophene)). Other potential large-area patterning routes are laser-induced thermal imaging[9] and reductive laser-induced bleaching[10]. The former method transfers the material from a precursor substrate to the desired locations by local heating/contact printing. In the latter case, a mixture of red- and green-emitting EL polymers embedded in a blue-emitting host was used. Selective bleaching yielded the three basic colours. Both processes are very delicate. In particular, laser-induced bleaching most probably suffers from relatively short lifetimes owing to the presence of large amounts of decomposition products.

In this paper we demonstrate a three-colour (RGB) OLED by solution processing using emitter polymers with photoresist properties, that is, soluble polymers, which can be cured photochemically to yield an insoluble form (polymer networks). In earlier work, we have successfully used the crosslinking of oxetane-functionalized hole-conductors for the fabrication of highly efficient blue OLEDs with three graded hole-injection layers[11,12]. Unlike other approaches in this direction using reactive side- or main-chain polymers with pendent polymerizable moieties[13–16] or monomers with several reactive groups[17–19], the use of oxetane reactive units is the only one so far that not only allows us to deposit an (in principle) unlimited number of layers[11], but simultaneously maintains the desired electrical and optical functionalities. Furthermore, the volume shrinkage is small and thus formation of microcracks upon curing is avoided. Here, we expand this approach to light-emissive polymers of the poly-spiro family[20].

The synthesis of the three oxetane-functionalized spirobifluorene-*co*-fluorene polymers emitting blue, green and red light (**P1**–**P3**) follows state-of-the-art procedure[20] and is depicted in Fig. 1. The monomer feed ratios used in the preparation of the polymers are given in Table 1. Thus, in the case of the blue-emitting polymer a true comparison between the crosslinkable polymer **P1** and the non-crosslinkable reference **P4** is possible, because monomer **3** is structurally very similar to monomer **2**, the only difference being the oxetane units. By contrast, no such comparison with their non-crosslinkable state-of-the-art analogues is possible for the green- and red-emitting crosslinkable polymers[20], because monomer **2** must replace some of the emissive moieties.

The polymerizations were achieved through a Suzuki polycondensation of the diboronic ester **1** and two or more aromatic dibromides (**2**–**7**) with 0.8 mol% of tetrakis-(triphenylphosphine)-palladium(0) as catalyst for 48 h at a temperature of 87 °C in a mixture of toluene (with some ethanol) and water with tri-potassium

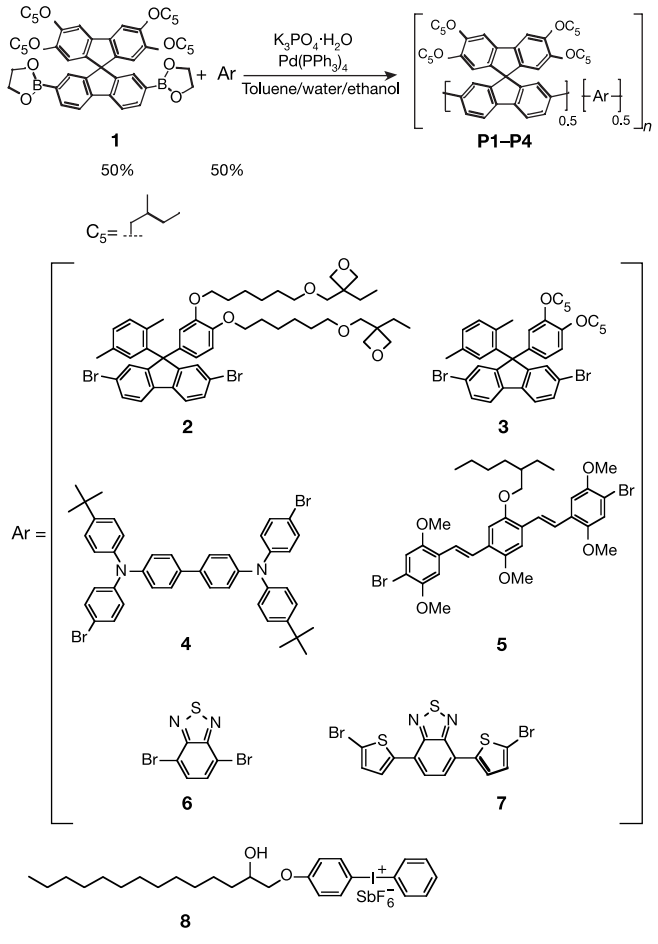

Figure 1 Synthesis of polymers **P1** to **P4**; chemical structure of photoacid **8**.

Table 1 **Composition and properties of the studied polymers**

	Colour-emitting polymers			
	P1 (X-blue)	P2 (X-green)	P3 (X-red)	P4 (blue)
1 Moiety (mol%)	50	50	50	50
2	25	25	25	–
3	15	–	–	40
4	10	10	10	10
5	–	15	–	–
6	–	–	10	–
7	–	–	5	–
M_w (g mol^{-1})	115,000	180,000	135,000	195,000
M_n (g mol^{-1})	48,000	47,000	55,000	72,000
$\lambda_{max,EL}$ (nm)	457	507	650	454
$\lambda_{max,abs}$ (nm)	399	392	394	397
CIE 1931 *x*	0.16	0.31	0.67	0.15
CIE 1931 *y*	0.19	0.58	0.33	0.16
η_{max} (pristine) (cd A^{-1})	2.9	7.0	1.0	3.0
U [V] at 100 cd m^{-2} (pristine)	4.5	3.8	8.3	4.6
η_{max} (crosslinked) (cd A^{-1})	3.0	6.5	1.1	n.a.
U [V] at 100 cd m^{-2} (crosslinked)	4.5	3.8	7.5	n.a.

Monomer feed ratio in the polymerization of the polymers (Fig. 1) and selected physical properties of the investigational polymers. n.a., not applicable. EL, electroluminescence; abs, absorbance; M_n, number average of molecular weight; M_w, weight average of molecular weight; $\lambda_{max,abs}$, maximum wavelength of absorption; $\lambda_{max,EL}$, maximum wavelength of electroluminescence; CIE 1931 x, y, colour coordinates according to the 1931 CIE convention; *U* [V] at 100 Cd m^{-1}, the voltage that needs to be applied in order to achieve 100 Cd m^{-1} light output; 'pristine' refers to non-crosslinked samples without addition of the photoacid **8**; X, crosslinkable.

phosphate as the base. It is another advantage of the oxetane functionality that it is chemically stable under these conditions. The polymers were obtained in yields of approximately 75% after precipitation in methanol and subsequent purification. The resulting conjugated polymers contain about 25 mol% of the oxetane-functionalized monomer **2** and are soluble in common organic solvents, such as toluene, tetrahydrofuran (THF) or xylene. The physical properties of these polymers are listed in Table 1.

Oxetanes are commonly polymerized cationically[21,22]. Therefore, to initiate the crosslinking process the photoacid **8** (Fig. 1) was added. Upon ultraviolet (UV) illumination, the initiator decomposes via a multiple-step mechanism and eventually generates protons H^+, which open the oxetane ring and start the polymerization[21]. Ultimately, the initially generated protons are consumed in the polymerization. After the softcuring step (see Methods) oxetane groups could no longer be detected by Fourier transform infrared (FTIR) investigations[11]. The chain end consists of an oxonium cation[23], so the crosslinked films were treated with solutions of various bases and nucleophiles for neutralization purposes. We found that rinsing the films with pure THF led to the best device performance. Further investigations are underway.

The electron-rich, highly fluorescent poly(spirobifluorene-*co*-fluorenes) are efficient photosensitizers, so in a competitive side reaction, radical cations are formed in the EL layer due to electron transfer between the polymer and the initiator. These cations effectively quench the EL. However, by a post-baking step at 180 °C, the EL can be completely recovered. The exact mechanism is currently under investigation and will be published elsewhere (C.D.M. and K.M., manuscript in preparation; ref. 21). We point out that with all three polymers, the emission spectra (photoluminescence (PL) as well as EL) were not affected by the crosslinking or the consecutive curing step.

OLED devices were prepared (see Methods for details) with the general structure: ITO/PEDOT (20 nm)/EL polymer (80 nm)/Ca (20 nm)/Ag (200 nm). In the non-crosslinked reference devices no photoinitiator **8** was added to the solution of the EL polymer.

In their non-crosslinked form, all three polymers show a performance that compares favourably with state-of-the-art EL polymers reported[20]. In particular, the blue-emitting polymer **P1** exhibits an excellent maximum efficiency of $\eta_{max} \approx 2.9\,cd\,A^{-1}$. This compares to $\eta_{max} \approx 3.0\,cd\,A^{-1}$ in the reference devices using non-crosslinkable **P4** (Table 1). The latter fact demonstrates that the incorporation of the oxetane groups did not significantly alter the EL properties of the resulting polymer.

The non-crosslinked polymers **P3** (red; $\eta_{max} \approx 1\,cd\,A^{-1}$) and **P2** (green; $\eta_{max} \approx 7\,cd\,A^{-1}$) exhibit somewhat reduced efficiency compared with previous non-crosslinkable examples (2.0 and 10.0 $cd\,A^{-1}$, respectively[20]). We attribute this (particularly in the red-emitting case) to an unfavourably changed charge-carrier balance in the polymer, resulting from the necessity of incorporating the oxetane-functionalized monomer **2** in 25% feed (partially replacing **6** and **7** in state-of-the-art analogues). Another reason for

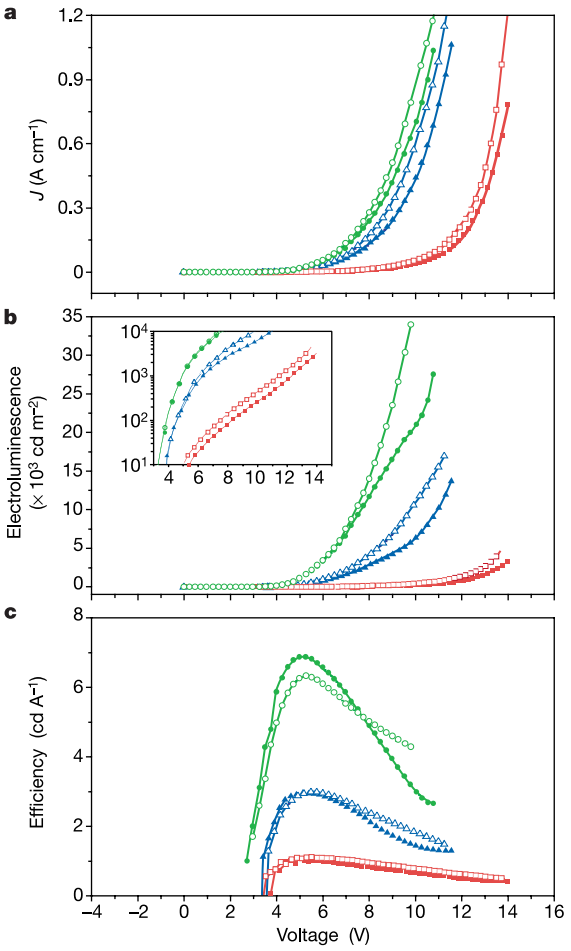

Figure 2 Performance of OLEDs based on crosslinkable polyspiro-derivatives. Voltage dependence of **a**, the current density *J*, **b**, the electroluminescence intensity, and **c**, the luminous efficiency for red-emitting (**P3**, squares), green-emitting (**P2**, circles), and blue-emitting (**P1**, triangles) devices. The open symbols refer to the crosslinked devices, the solid symbols to the non-crosslinked reference devices. The lines are guides to the eye. The inset of **b** shows the same data sets as the main figure, however, on a semi-logarithmic scale.

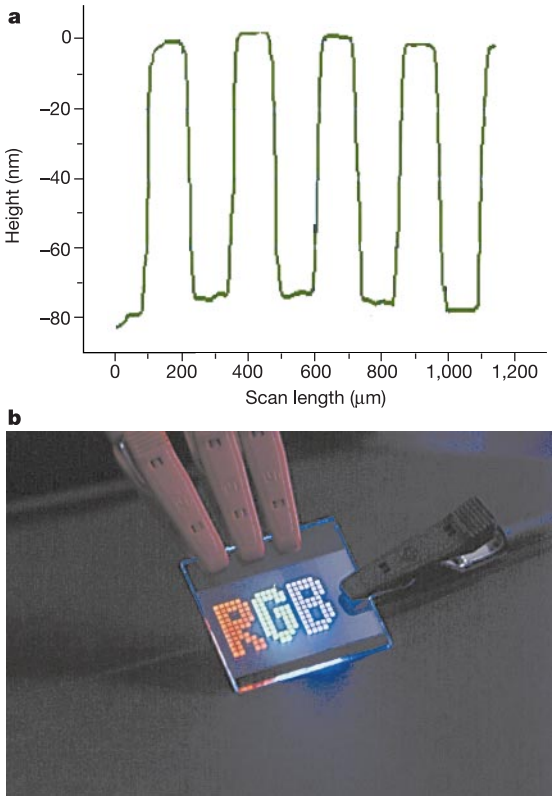

Figure 3 Demonstration of the photoresist properties of crosslinkable polyspiro-derivatives. **a**, Cross-section of a 73-nm-thick photo-structured layer of the blue emitting polymer (**P1**) illuminated through a grid with 250-μm spacing (125-μm openings). **b**, Photograph of a RGB (red, green, blue) device. Dimensions of the glass substrate are 25 × 25 mm.

the reduced performance is probably the use of calcium cathodes in this work as opposed to barium in ref. 20.

The OLEDs made from crosslinked **P1** and **P3** exhibited identical, if not even slightly improved maximum efficiency η_{max} compared to the non-crosslinked references (Fig. 2; see also Table 1). In contrast, OLEDs made with the crosslinked green-emitting **P2** achieved only about 92% of the non-crosslinked analogues. The turn-on voltage for light emission was slightly reduced in all crosslinked devices. Furthermore, in all three cases the crosslinked devices exhibited higher efficiency at high luminance, and they could be driven to higher current density before breakdown occurred.

After having demonstrated the ability to crosslink the materials without significant alteration of their EL properties, we then took advantage of the photoresist-type properties of the materials and investigated the possibility of photo-patterning the films. For this purpose, the layers were irradiated through a shadow mask (grating; 250-μm period, 125-μm gap size). After curing, the films were developed by immersing them into THF, which re-dissolved the non-irradiated areas of the film. The line scan obtained with a profilometer (Fig. 3a) clearly demonstrated the formation of 125-μm-wide ridges with a height identical to the previous film thickness (that is, full modulation). The edges are sharp, demonstrating that no significant diffusion of the photogenerated protons into the dark regions takes place. We point out that the achievable resolution in our materials is much higher (a few micrometres), as was tested by illuminating with a holographic interference pattern (E. Mecher, C.D.M. and K.M., manuscript in preparation). By applying the above-mentioned procedure three times, once for each polymer, we were able to fabricate pixelated devices with three individually addressable colours (Fig. 3b).

In conclusion, we have demonstrated a RGB polymer OLED obtained by simple spin-coating. Except for the blue-emitting material the efficiencies of the new generation of EL polymers do not reach the best state-of-the-art values quite yet, but this can certainly be achieved by optimizing the synthetic route. Coatings were obtained that can be processed similarly to ordinary photoresists using standard lithographic techniques. We believe this to be a highly promising technology for the fabrication of true-colour matrix displays with many advantages, such as thermal and/or mechanical robustness (due to the formation of polymer networks) and higher efficiency at high light levels than their non-crosslinked counterparts. □

Methods

Film preparation

Thin films were prepared by spin-coating the polymers from toluene solution (15 mg ml^{-1}), which additionally contained 0.5 wt% (relative to EL polymer) of the photoacid {4-[(2-hydroxytetradecyl)-oxyl]-phenyl}-phenyliodonium hexafluorantimonate **8** (Fig. 1) as initiator for the cationic polymerization of the oxetane units[21]. The films were irradiated (standard handheld UV lamp, UV B, $\lambda = 302$ nm) for about 3 s in inert gas atmosphere at room temperature. Afterwards, to further advance the crosslinking process in the growing network, the films were annealed at 90 °C for 30 s ('soft curing'). The heating increased the diffusional mobility of the oxetane reactive groups and thus the degree of crosslinking. Afterwards, the films were rinsed with THF and finally heated to 180 °C for 5 min to remove the radical cations formed upon polymerization ('post baking'). The resulting polymer networks were found to be insoluble in any common solvent. The films exhibited an average surface roughness (root mean square, r.m.s.) of <1 nm as determined by atomic-force microscopy (AFM). No signs of shrinkage were found.

Device preparation and physical characterization

ITO (indium tin oxide)-coated glass substrates were commercially obtained from Merck display glass (20 Ω inch^{-2}) and carefully cleaned and dried before use. An ozone treatment yielded a rather hydrophilic surface.

Single-colour OLED devices were obtained by first spin-coating PEDOT as the hole-injecting contact (20 nm), baking at 120 °C, followed by spin-coating of the polymers from toluene solution (15 mg ml^{-1}) to yield 80-nm-thin films, then crosslinking the films as described above, and finally depositing Ca (20 nm) and Ag (200 nm) as the top electrode (active area 0.08 cm^2). Except for the PEDOT deposition, all other steps were performed in a glove box under inert gas atmosphere.

RGB devices were fabricated by depositing the first polymer as described above, illuminating selected areas through a shadow mask, soft curing, then removing the still soluble, non-illuminated areas with THF. This procedure was repeated for each colour, and finally the devices were post-baked. The results were independent of the sequence of deposition of the three colours, unambiguously demonstrating that a layer once crosslinked is unaffected by the others (no inter-diffusion/penetration).

The characterization of the devices was performed by a custom-made voltage generator using a calibrated amperemeter and a calibrated photo diode.

Chemicals

All chemicals were purchased from Aldrich, Lancaster, or Strem and were used without further purification. Monomers **1** and **3–7** were synthesized as described; see ref. 24. The reactions were carried out under an argon atmosphere. Solvents were commercial pro analysis (p.a.) quality.

Synthesis of 2

Synthesis of 2,7-dibromo-9-(2,5-dimethylphenyl)-9-(3,4-di(3-ethyl(oxetane-3-ethyloxy)-hexyloxyphenyl))-fluorene was carried out as follows:

1 g (1.9 mmol) of 2,7-dibromo-9-(2,5-dimethylphenyl)-9-(3,4-dihydroxyphenyl)-fluorene was dissolved in 10 ml dimethyl sulphoxide (DMSO) in a 100-ml Schlenk flask under nitrogen atmosphere. 2.08 g (7.5 mmol, 4 equiv.) 3-(6-bromohexylmethyl)-3-ethyloxetane were added under stirring. The mixture was degassed several times. 0.49 g (7.5 mmol, 4 equiv.) of very fine ground KOH were added. The reaction was performed at 60 °C. After 5 h the mixture was cooled to room temperature and diluted with 20 ml water. The aqueous phase was extracted with ether. The organic phases were collected and dried over anhydrous magnesium sulphate. After removing the solvent the resulting oil was purified by silica-gel column chromatography using toluene/ethylacetate (4:1) as eluent. The product **2** was obtained as a light yellow oil in 67.8% yield.

^{1}H NMR ($CDCl_3$) spectrum: 7.66–6.48 (multiplet (m), 12H, aromatic); 4.45–4.30 (m, 8H, -O$\underline{CH_2}$-oxetane); 3.95–3.80 (m, 4H, -O$\underline{CH_2}$-ether); 3,49 (singlet (s), 2H, -O$\underline{CH_2}$-); 3,48 (s, 2H, -O$\underline{CH_2}$-); 3.42 (triplet (t), 4H, -O$\underline{CH_2}$-); 2.19 (s, 6H, benzylic); 1.82–1.29 (m, 20H, aliphatic); 0.89–0.79 (m, 6H, -CH_3).

General procedure for polymer synthesis

The boronic ester **1** (3.203 g, 4.0 mmol), the mixture of bromide monomers **2–7** (see Table 1; 4.0 mmol in total), and $K_3PO_4 \cdot H_2O$ (4.05 g, 17.6 mmol) were added to a mixture of toluene (12 ml), water (6 ml) and ethanol (0.1 ml), and the solution was degassed for 30 min. $Pd(PPh_3)_4$ (70 mg, 0.06 mmol) was added, and the suspension was heated under reflux (~87 °C) under argon with vigorous stirring. After 2 days boronic ester (0.03 g, 0.058 mmol) was added, and the mixture was refluxed for a further 6 h. Then bromobenzene (0.05 ml, 0.47 mmol) was added for endcapping and the mixture refluxed for a further 3 h. After cooling, the reaction mixture was diluted with toluene (80 ml) and stirred with NaCN (2% in water, 100 ml) for 3 h. The organic phase was separated, washed with water and poured into methanol to precipitate the polymer. This was then dissolved in THF (80 ml) and reprecipitated in methanol (200 ml). The polymer was collected by filtration and dried under vacuum. The later procedure was repeated.

Yield of **P1**: 4.3 g, 77%. ^{1}H NMR ($CDCl_3$) spectrum: 7.8–6.6 (m, 22.1H); 6.4–6.0 (m, 2H, Spiro); 4.3–4.4 (m, 4H, OCH_2-oxetane); 4.0–3.3 (2 × m, 15.2H, OCH_2); 2.2–0.7 (m, 61.6 alkyl H).

Yield of **P2**: 2.0 g, 76%. ^{1}H NMR ($CDCl_3$) spectrum: 7.8–6.6 (m, 21.8 H); 6.4–6.0 (m, 2H, Spiro); 4.3–4.4 (m, 4H, OCH_2-oxetane); 4.0–3.3 (2 × m, 19.0H, OCH_2); 2.2–0.7 (m, 60.1 alkyl H).

Yield of **P3**: 1.96 g, 75%. ^{1}H NMR ($CDCl_3$) spectrum: 7.8–6.6 (m, 19.8H); 6.4–6.0 (m, 2H, Spiro); 4.3–4.4 (m, 4H, OCH_2-oxetane); 4.0–3.3 (2 × m, 14.0H, OCH_2); 2.2–0.7 (m, 55.6 alkyl H).

Yield of **P4**: 3.79 g, 79%. ^{1}H NMR ($CDCl_3$) spectrum: 7.8–6.2 (m, 20.4H); 6.2–6.1 (m, 4H, Spiro); 4.0–3.4 (2 × m, 11.2H, OCH_2); 2.1–0.7 (m, 58.8H, alkyl H).

Received 7 October; accepted 31 December 2002; doi:10.1038/nature01390.

1. Friend, R. H. *et al.* Electroluminescence in conjugated polymers. *Nature* **397,** 121–128 (1999).
2. Heeger, A. J. Light emission from semiconducting polymers: light-emitting diodes, light-emitting electrochemical cells, lasers and white light for the future. *Solid State Commun.* **107,** 673–679 (1998).
3. Kraft, A., Grimsdale, A. C. & Holmes, A. B. *Angew. Chem. Int. Edn* **37,** 402–428 (1998).
4. Salbeck, J. Electroluminescence with organic compounds. *Ber. Bunsenges. Phys. Chem.* **100,** 1667–1677 (1996).
5. Pardo, D. A., Jabbour, G. E. & Peyghambarian, N. Application of screen printing in the fabrication of organic light-emitting devices. *Adv. Mater.* **12,** 1249–1252 (2000).
6. Birnstock, J. *et al.* Screen-printed passive matrix displays based on light-emitting polymers. *Appl. Phys. Lett.* **78,** 3905–3907 (2001).
7. Birnstock, J. *et al.* Screen-printed passive matrix displays and multicolor devices. *Proc. SPIE* **4464,** 68–73 (2001).
8. Haskal, E. *et al.* Ink jet printing of passive matrix polymer light-emitting displays. *SID Digest Tech. Pap.* **33,** 776–779 (2002).
9. Seong, T. L. *et al.* A new patterning method for full-colour light-emitting diodes: laser-induced thermal imaging. *SID Digest Tech. Pap.* **33,** 784–787 (2002).
10. Trattnig, C., Pogantsch, A., Langer, G., Kern, W. & Zojer, E. Polymer-based red, green and blue emitting devices fabricated by reductive photopatterning. *Appl. Phys. Lett.* **81,** 4269–4271 (2002).
11. Müller, D. C. *et al.* Efficient blue organic light-emitting diodes with graded hole-transport layers. *ChemPhysChem* **1,** 207–211 (2000).
12. Bayerl, M. S. *et al.* Cross-linkable hole transport materials—Preparation of multilayer organic light-emitting diodes by spincoating. *Macromol. Rapid Commun.* **20,** 224–227 (1999).
13. Li, X. C. *et al.* A blue light emitting copolymer with charge transporting and photo-crosslinkable functional units. *Synth. Met.* **84,** 437–438 (1997).

14. Le Barney, P., Bouche, C. M., Facoetti, H., Soyer, F. & Robin, P. Synthesis of side chain electroluminescent polymers and properties of devices including them. *Proc. SPIE* **3148,** 160–169 (1997).
15. Bellmann, E. *et al.* New triarylamine-containing polymers as hole transport materials in organic light-emitting diodes: effect of polymer structure and crosslinking on device characteristics. *Chem. Mater.* **10,** 1668–1676 (1998).
16. Jiang, X., Liu, S., Ma, H. & Jen, A. K. High-performance blue light-emitting diode based on a binaphthyl-containing polyfluorene. *Appl. Phys. Lett.* **76,** 1813–1815 (2000).
17. Bacher, A. *et al.* Photo-cross-linked triphenylenes as novel insoluble hole transport materials in organic LEDs. *Macromolecules* **32,** 4551–4557 (1999).
18. Li, W. *et al.* Covalently interlinked organic LED transport layers via spin-coating/siloxane condensation. *Adv. Mater.* **11,** 730–734 (1999).
19. Chen, J. P. *et al.* Efficient, blue light-emitting diodes using cross-linked layers of polymeric arylamine and fluorene. *Synth. Met.* **107,** 129–135 (1999).
20. Becker, H., Heun, S., Treacher, K., Büsing, A. & Falcou, A. Materials and inks for full-colour PLED displays. *SID Digest Tech. Pap.* **33,** 780–782 (2002).
21. Fouassier, J-P. *Photoinitiation, Photopolymerization, and Photocuring: Fundamentals and Applications* 102–144 (Hanser/Gardner, Cincinnati, 1995).
22. Sasaki, H. & Crivello, J. V. The synthesis, characterization, and photoinitiated cationic polymerization of difunctional oxetanes. *J. Macromol. Sci. A* **29,** 915–930 (1992).
23. Penczek, S. & Kubisa, P. in *Comprehensive Polymer Science* (ed. Allen, G.) Vol. III, 751–786 (Pergamon, Oxford, 1989).
24. Treacher, K. *et al.* Conjugated polymers containing spirobifluorene units and fluorene units, and the use thereof. German patent application DE 2001-10114477; WO 2002-077060.

Acknowledgements Partial financial support was granted by the Deutsche Forschungsgemeinschaft, the Bundesministerium für Bildung und Forschung, the Fonds der Chemischen Industrie (Kekule grant for N.R.), and the Bavarian government through 'Neue Werkstoffe'.

Competing interests statement The authors declare that they have no competing financial interests.

Correspondence and requests for materials should be addressed to K.M. (e-mail: klaus.meerholz@uni-koeln.de).

Precise dating of Dansgaard–Oeschger climate oscillations in western Europe from stalagmite data

D. Genty*, D. Blamart*, R. Ouahdi*, M. Gilmour†, A. Baker‡, J. Jouzel* & Sandra Van-Exter§

* *IPSL/Laboratoire des Sciences du Climat et de l'Environnement, UMR CEA/CNRS 1572 Bat. 709, L'Orme des Merisiers CEA Saclay, 91191 Gif sur Yvette cedex, France*
† *The Open University, Department of Earth Sciences, Uranium Series Facility, Milton Keynes MK7 6AA, UK*
‡ *Centre for Land Use and Water Resources Research, University of Newcastle upon Tyne, Newcastle upon Tyne NE1 7RU, UK*
§ *University of Montpellier, Laboratoire Hydrosciences, UMR 5569 (CNRS-UM2-IRD), Maison des sciences de l'eau, CC 057, Place E. Bataillon, 34095 Montpellier cedex 5, France*

The signature of Dansgaard–Oeschger events—millennial-scale abrupt climate oscillations during the last glacial period—is well established in ice cores and marine records[1–3]. But the effects of such events in continental settings are not as clear, and their absolute chronology is uncertain beyond the limit of ^{14}C dating and annual layer counting for marine records and ice cores, respectively. Here we present carbon and oxygen isotope records from a stalagmite collected in southwest France which have been precisely dated using ^{234}U/^{230}Th ratios. We find rapid climate oscillations coincident with the established Dansgaard–Oeschger events between 83,000 and 32,000 years ago in both isotope records. The oxygen isotope signature is similar to a record from Soreq cave, Israel[4], and deep-sea records[5,6], indicating the large spatial scale of the climate oscillations. The signal in the carbon isotopes gives evidence of drastic and rapid vegetation changes in western Europe, an important site in human cultural evolution. We also find evidence for a long phase of extremely cold climate in southwest France between 61.2 ± 0.6 and 67.4 ± 0.9 kyr ago.

Several of the 24 Dansgaard–Oeschger (DO) events identified in the GRIP[7,8] and GISP2[9] Greenland ice cores over the last glacial period indicate air temperature changes greater than 10 °C. North Atlantic and Mediterranean marine cores show similar amplitude changes in the water temperature[5,10,11]. However, the consequences of these events on the continent are still not well known, because of the scarcity of well-preserved and well-dated records. We know that the ocean–atmosphere system was closely coupled as far as the central Mediterranean region, where the vegetation has been reconstructed thanks to pollen records (in lakes) that reacted very quickly and sensitively to these abrupt climate changes[12,13]. GRIP and GISP2 dating uncertainties may exceed the duration of a single DO event for a large part of the glacial period (estimated for GISP2 at 2% over the past 40 kyr, and between 5% and 10% for the period <50 kyr ago[14,15]). Marine cores are dated by orbital tuning with inherent accuracy and, for their late-glacial part, by ^{14}C dating. However, for periods of interest here, this latter method suffers from limitations linked with analytical precision, ^{14}C age calibration, fluctuations in the carbon cycle, and a varying age reservoir[16]. The few continental records also display a lack of absolute ages, especially after 40 kyr ago[12,13]. This highlights the importance of establishing chronologies of those events from other records.

Here we present stable isotope records (δ^{13}C and δ^{18}O) from a stalagmite of the Villars cave (southwest France, less than 200 km from the Atlantic Ocean; Fig. 1) that show most of the DO events between 83 and 32 kyr ago (Fig. 2). We have determined 27 thermal ionization mass spectrometry (TIMS) U-series dates on this 147-cm-long stalagmite ('Vil9'), leading to an absolute timescale with errors less than 2% (2σ) up to 83 kyr ago (see Supplementary Table 1 for information, and ref. 17 for methods). Three main hiatuses occurred at 78.8–75.5 kyr ago (referred to as D2), 67.4–61.2 kyr ago (D3) and 55.7–51.8 kyr ago (D4). The regular δ^{13}C and δ^{18}O decreases towards the D3 hiatus, and also the steady increase that is observed afterwards, suggests that this growth cessation is

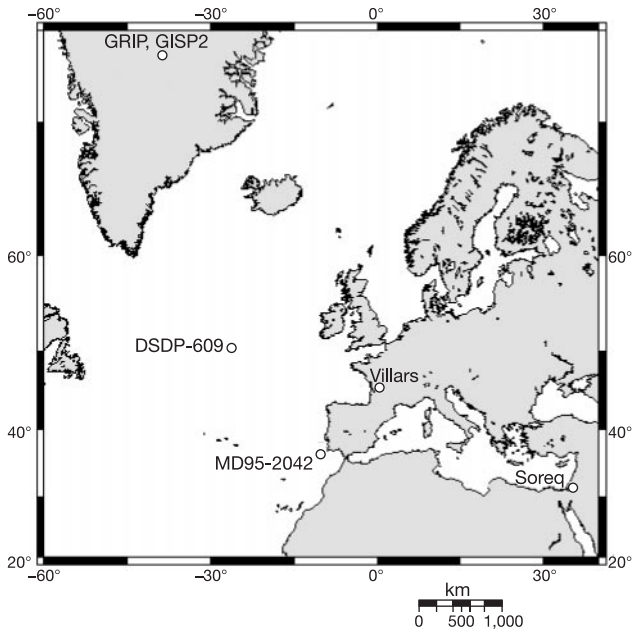

Figure 1 Map showing locations of the study sites. GRIP and GISP2; 72.58° N, 37.64° W. Villars cave; 45.30° N, 0.50° E. MD95-2042; 37.48° N, 10.10° W. DSDP 609; 50° N, 27° W. Soreq cave; 31.6° N, 35° E.